EXPERIMENTAL & CLINICAL
Cardiology

EXPERIMENTAL & CLINICAL CARDIOLOGY

Volume 20, Issue 11, 2014

Title: "An Approach for Physiological Motion Compensation in Robotic-Assisted Cardiac Surgery"

Authors: Angelica I. Aviles, Pilar Sobrevilla and Alicia Casals

How to reference: An Approach for Physiological Motion Compensation in Robotic-Assisted Cardiac Surgery/Angelica I. Aviles, Pilar Sobrevilla and Alicia Casals/Exp Clin Cardiol Vol 20 Issue11 pages 6713-6724 / 2014

An Approach for Physiological Motion Compensation in Robotic-Assisted Cardiac Surgery

Angelica I. Aviles*, Pilar Sobrevilla†, and Alicia Casals‡

* Intelligent Robotics and Systems Group, Universitat Politécnica de Cataluya, Barcelona, Spain.
† P. Sobrevilla, Department of Applied Mathematics II, Universitat Politécnica de Cataluya, Barcelona, Spain.
‡ A. Casals, Institute for Bioengineering of Catalonia and Universitat Politécnica de Cataluya, Barcelona, Spain.
{angelica.ivone.aviles, pilar.sobrevilla, alicia.casals}@upc.edu

Abstract—The lack of physiological motion compensation is a major problem in robotic-assisted cardiac surgery. Since the heart is beating while the surgeon carried out the procedure, dexterity of the surgeon's and precision are compromised. Due to the operative space and the visibility of the surgical field are reduced, the most practical solution is the use of computer vision techniques. The lack of efficiency and robustness of the existing proposals make physiological motion compensation to be considered an open problem. In this work a novel solution to solve this problem based on the minimization of an energy functional is presented. It is described in the three-dimensional space using the $\ell 1-$regularized optimization class in which cubic b-splines are used to represent the changes produced on the heart surface. Moreover, the logarithmic barrier function is applied to create an approximation of the total energy in order to avoid its non-differentiability. According to the results, this proposal is able to deal with complex deformations, requires a short computational time and gives a small error.

Keywords—Beating heart surgery, image analysis, motion compensation

1. Introduction

Minimally invasive cardiac surgery (MICS) has become a popular approach since it offers different benefits in comparison with traditional cardiac surgery such as [1]: smaller incisions; shorter term rehabilitation; less bleeding; faster recovery; reduction of blood transfusion and cosmetic improvement. Despite all benefits during a MICS, surgeon has to deal with important difficulties, among which it must be highlighted the following [2], [3]: reduction of the operative space; lessening in surgical field visibility; loss of mobility and lack of comfort (ergonomic challenges). Apart from overcoming previous drawbacks, Robotic-Assisted Cardiac Surgery has emerged as a very practical and suitable solution to MICS because improves surgeon's dexterity and precision, eliminates the tremor and avoids fatigue. However, since the heart is beating while intervention is carried out, the surgeon has to tackle two sources of disturbances: respiration and heartbeat. These physiological motions hinder surgeon's gestures and limit precision during surgery. Thus, a research goal is to compensate them in order to provide the surgeon with the sensation of working in a motionless area.

To cope with physiological motion compensation problem some authors [4], [5], [6], [7] have proposed the use of mechanical stabilization devices, which are positioned over the heart surface to keep the region of interest in steady state. However, their performances have been reported to be unsatisfying. The main drawbacks of this type of devices are that exhibit $1.5-2.4$mm of residual motion (i.e. heart motion still needs to be manually compensated by the surgeons), they can only be applied on the top of the heart surface, and they can damage the heart tissue, and affect the mechanical performance of the heart [8], [9]. Likewise, active cardiac stabilizers are proposed in [10], [11], wherein suppression of residual motion is seen as vibration cancelation. Although authors proved the viability of using this type of stabilizers,

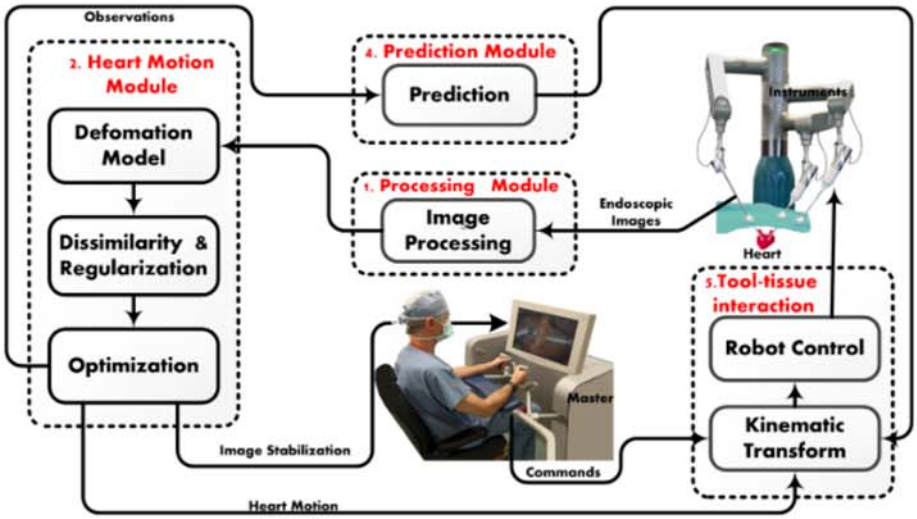

Fig. 1: Proposed solution for motion compensation in robotic-assisted heart surgery.

besides their size and their long-term stability, the fact that biocompatibility issues are not taken into account, make still complicated the use of this type of devices in real clinical environments. A different approach was explored in [12], [13]; where the use of predictive control to compensate physiological motion is put forward. However some problems related to noise and the lack of efficient motion retrieval restrict the use of this kind of approach.

In order to avoid the above-mentioned drawbacks, Nakamura et al. [14] demonstrated the feasibility and practicality of using Computer Vision Techniques (CVT) for heart motion compensation. In that work authors, introduced the concept of heart synchronization and developed a system which artificial markers were used for tracking a region of interest. Artificial markers were also used in [15] for motion estimation using a calibrated vision system. However, authors pointed out the limitations of using those markers and proposed replace them by texture information. Likewise, artificial markers and the physical properties of the heart were adopted in [16] for tracking the beating heart. Although an additional sensor was also used to measure the pressure inside the ventricle, it was proved that was a disadvantage due to the reduced operating space. In [17] physics-based heart motion tracking method is proposed, where heart surface is described as a physical elastic body in form of Partial Differential Equation (PDE). In their work authors attached passive colored markers to the heart to carry out the feature extraction. Previous proposals are unpractical due to the difficulty of placing artificial markers on the heart surface due to its glossy property, the reduced work space, the blood and vapors.

To avoid the limitations arising from the use of artificial markers, Ortmaier et al. [18] suggested employing natural markers of the heart for tracking the heart motion. In that work, an affine motion model was used for tracking the motion of the 2D projection of the beating-heart. In [19] the combination of maximally stable extremal regions (MSER) and the traditional gradient based image features was used for salient landmark selection. Moreover, the authors extend the Lucas-Kanade (LK) method to achieve temporal tracking of the heart. Later on authors in [20] proposed the use of a probabilistic framework based on Markov-Random Field - Bayesian Network (MRF-BN) for tissue deformation recovery. Another tracking method is presented in [21], in which authors pointed out the introduction of Thin- Plate Splines (TPS) for representing the heart surface deformation, and proposed the use of a dual Fourier series to predict the heart motion during occlusions. The approach proposed in [22] makes use of the SURF method for recovering distinct regions that are used in the Lucas-Kanade tracker. A template matching method using stereoscopic fluorescence images is implemented in [23], in which the normalized cross-correlation (NCC)

method is used. In a most recent work [24], a tracking scheme that uses a probabilistic similarity measure is proposed. In that work the joint spatial-color distribution is applied to represent the target region, and TPS are used for recovering 3D information. Unfortunately, a major problem of the existing robotic surgery systems is the lack of physiological motion compensation. Although different solutions have been presented; the lack of robustness, efficiency and accuracy lead this problem to be considered still open [25].

In this work, a 3D tracking based on the $\ell 1-$regularized optimization class is presented. To the best of our knowledge, there are no previous reports of using this class in the context of physiological motion compensation. Moreover, the use of explicit regularization is highlighted which allows stabilizing the solution and decreasing the number of local minima.

This paper is organized as follows. In Section 2 the general problem to be solved is presented as a total energy minimization issue. The main stages of the proposed solution are described in Section 3. Then, some results are presented at Section 4, and the conclusions are put forward in Section 5. The paper concludes with a list of notation terms used along the work.

2. Problem Statement

The setup for heart motion compensation is part of the Robotic Surgical System given in Fig. 1., in which four modules are integrated in a robotic surgical system. Apart from the heart motion compensation module the system includes: an image processing module which allows the correction and enhancement of the image sequence; a prediction module which guarantees system operation even in presence of occlusions given by the surgical instruments and blood; and a tool-tissue interaction module, which synchronizes the heart motion and instruments avoiding tissue damage.

Heart motion compensation can be formulated as an energy optimization problem, wherein information source is given by a stereo camera that allows reconstructing the three-dimensional world space (see Fig. 2). So, the general idea is that, once the region of

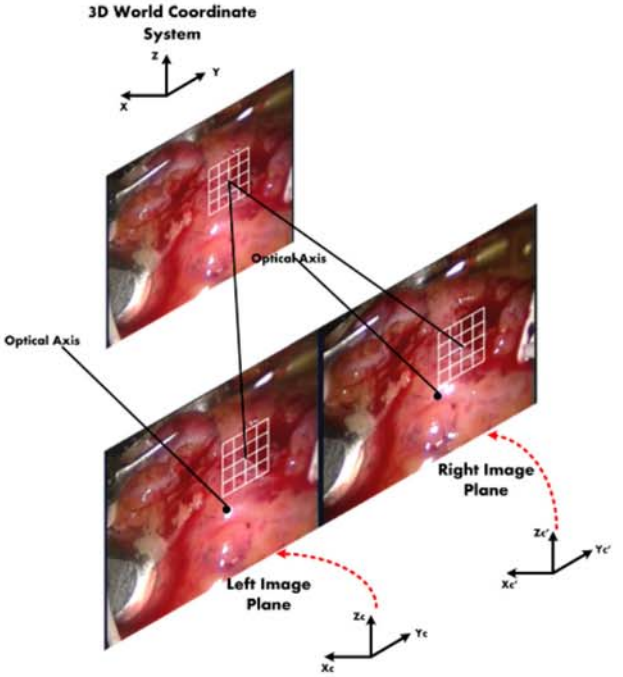

Fig. 2: The points in the three dimensional space world are obtained as the projections of the corresponding points of the left and right images.

interest to be repaired (i.e. the artery) is identified, its deformation, is controlled by the changes measured in a set of uniformly spaced set of points, $\mathbf{P}$, at each instant time, t. Thus, if $I_L : \Omega_{I_L} \rightarrow \mathbb{R}$ and $I_R : \Omega_{I_R} \rightarrow \mathbb{R}$ are rectified images of the left and right camera two terms have to be considered: i) a measure of discrepancy, E_D, between I_L and I_R images and ii) a regularization term, E_R, that allows restricting the space of solutions. Then, the total energy, E_t, given by the following generalized equation:

$$E_t(\mathbf{P}) = E_D(\mathbf{I_L}(\mathbf{d}(x;\mathbf{P}) + x), \mathbf{I_R}(x)) + \zeta E_R(\mathbf{d}(x;\mathbf{P})) \quad (1)$$

where $\zeta \in \Re^+$ gives a balance between both terms, and $\mathbf{x}$ represents a vector in $\Re^n$. Given equation 1, for solving the heart motion compensation problem, in addition to selecting the optimization method, it is necessary to choose both the discrepancy measure and the regularization method that must be used in order to obtain the better solution. Moreover, there are other factors to be taken into account that com-

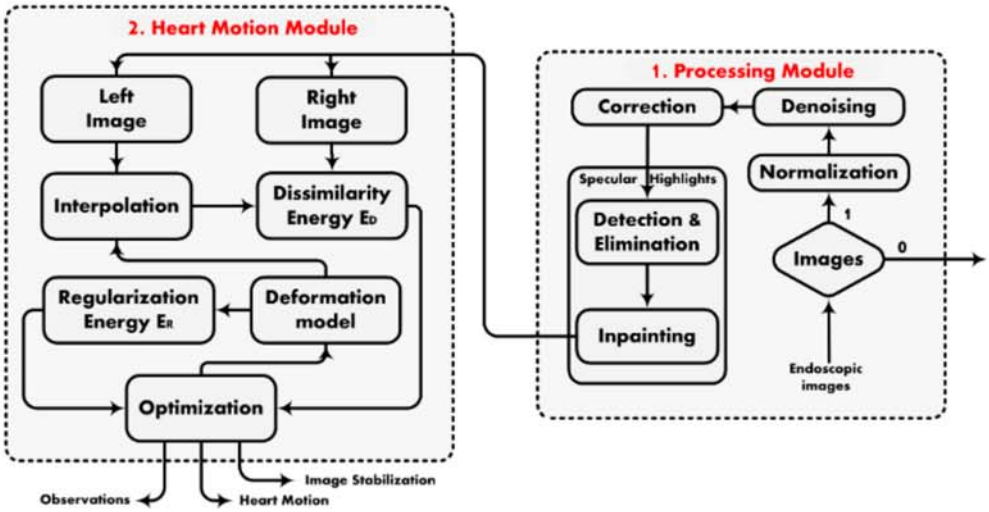

Fig. 3: Detailed flow chart of the Processing Module and the Heart Motion Module.

plicate the problem solving. there are Firstly, there are the *precision* requirements imposed by the small blood vessels diameter (between 0.5 mm and 2.0). Furthermore, illumination issues must be born in mind. On the one hand, due to the glossy property of the heart surface, *specular highlights* appear during the intervention. They have to be taken into account since they are a source of error and cause loss of information. On the other hand, due to the source of illumination is not fixed *illumination variance* is expected. Thus, in order to increase robustness the solution has to work in a lighting-insensitive scenario. Moreover, in order to avoid introducing error in the solutions, *undesirable singularities* (i.e. occlusions) must be taken into consideration.

3. Proposed Solution

In this section, the solution for compensating physiological motion during a Robotic-Assisted cardiac surgery is presented. Firstly, the selection of the deformation model which allows parametrizing the changes on the heart surface is presented. Secondly, explanation about how the Eq. 1 is reformulated. That is, the definition of the two terms, E_D and E_R, of our energy functional will be presented. Since both are formulated using $\ell 1-$norm the expression defined is given via $\ell 1-$regularized optimization class. Then, an explanation about how specular highlights are detected and removed is presented, this process is carried out in order to increase robustness and efficiency of the proposed solution. For a better understanding of how these three steps are correlated a flowchart is depicted in Fig. 3.

3.1 Deformation Mapping

In order to paramatrize the heart motion, a deformation model is needed. Although there are several models, the selected model for this application must meet two characteristics: short computational time and offer valuable information [26]. A well-defined classification of deformation models can be found in [27], in which three categories are described based on if are: i) inspired by physical models, ii) knowledge-based models or iii) inspired by approximation and interpolation models. Although models of the first category have been widely applied in medical applications, these are inherently computationally expensive and have difficulties for dealing with complex deformations (i.e. provide inaccurate deformation) [28]. On the other hand, even though in the second category are able of dealing with complex deformations their computational complexity makes them unsuitable to be used in this area. Therefore, the third category has been selected since models in this category offer a good trade-off between computational time and ability of dealing with complex deformations, offering valuable information during the image transformation.

In the third category well-known models can be found as: thin-plate splines [29], elastic body splines [30], piecewise affine [31] among others. The main drawbacks of these models are: inverse inconsistency; lack of mathematical optimality and continuity; and high computational demand. Another option in this category is B-splines that offer various desirable benefits such as [32], [33]: easy manipulation; compact support; low computational cost; optimal mathematical properties; multiresolution; Hölder continuous of order n; affine invariance and preservation of both convexity and diminishing properties. Given the advantages of B-splines (free-forms) they have been selected as the deformation model used for measuring the disparity $\mathbf{d}$. Particulary, in this work we have considered b-splines of degree 3 (i.e. cubic), whereby is defined as follows:

$$\mathbf{d}(x,\mathbf{P}) = \sum_{j_1=0}^{3} ... \sum_{j_d=0}^{3} \mathbf{P}_{j_1,...,j_d} \prod_{k=1}^{n} \Upsilon_k(u_k) : \{x \in \mathbb{R}^n\} \tag{2}$$

Let $\mathbf{C_j} \mid \mathbf{C_j} \geq 0$ be all control points in d-dimensions belonging to a lattice uniformly spaced. Moreover, defining $\Upsilon_{k,m}$ as basis functions given by

$$\begin{aligned} \Upsilon_0(\mu) &= (1-\mu)^3/6 \\ \Upsilon_1(\mu) &= (4+3\mu^3-6\mu^2)/6 \\ \Upsilon_2(\mu) &= (1-3\mu^3-3\mu^2+3\mu)/6 \\ \Upsilon_3(\mu) &= \mu^3/6 \end{aligned} \tag{3}$$

Once d is determined, the distance along the Z-axis is retrieved by:

$$Z = \frac{\mathfrak{f} * \mathfrak{B}}{d_m} \tag{4}$$

where $\mathfrak{f}$ is the focal length and $\mathfrak{B}$ the baseline.

3.2 The Discretize-Optimize Approach

As the physiological motion compensation problem is here treated as an energy minimization problem, the main difficulties are twofold: (i) the definition of the energy terms that represent adequately the problem to be solved, and (ii) how to efficiently represent each term of the energy functional. Thus, in this section, these two issues are described. Moreover, although existing proposals are oriented to use the $\ell 2-$ norm, in this section, the solution is described using the $\ell 1-$regularized optimization class. This has been the chosen regularization class because, besides outperforming the solutions obtained using the $\ell 2-$ norm, the $\ell 1-$ norm: works-well with outliers, is related to robustness, outperforms solutions obtained by the $\ell 2-$ norm and is non-sensitivity to changes of intensity. In addition, it should be emphasized that the aim of using explicit regularization in this application is threefold: guarantee an existing and stable solution via restriction of the space of solutions; to penalize oscillating deformations (i.e. generate a well-defined displacement field); and decrease the computational cost of the optimization process.

To reformulate Eq. 1, firstly, it is necessary to evaluate the discrepancy between the two images. Although different methods can be considered, the selection of the most adequate depends on the problem to be solved. In here, since the images are acquired by the same sensor, big intensity variations between them are not expected. Therefore, an iconic method is a perfect match for this application. In particular, to reformulate E_D, the Sum of Absolute Differences (SAD) method has been selected due to its simplicity, low computational time working in real-time, and robustness in front of variation of intensities and outliers.

Secondly, as undesirable mathematical properties appear, they lead us to deal with an ill-posed problem. This kind of problem is characterized by the fact that it does not fulfill the Hadamards postulate [34], which asserts that a well-posed problem must satisfy three main requirements: i) existence, ii) uniqueness and iii) continuity. Thus, it is necessary to define the penalization term, E_R, in order to impose stability to the solution and decrease the number of local minima. Although there are various options for choosing E_R such as: the well-known method called Tikhonov [35], Mumford and Shah model [36], curvature among others, they have disadvantages such as lack of edge preservation, complex analysis or negative practical results lead us to select the method proposed by Rudin et al. called Total Variation (TV) [37]. Thus, using both SAD and TV methods Eq. 1 is rewritten as

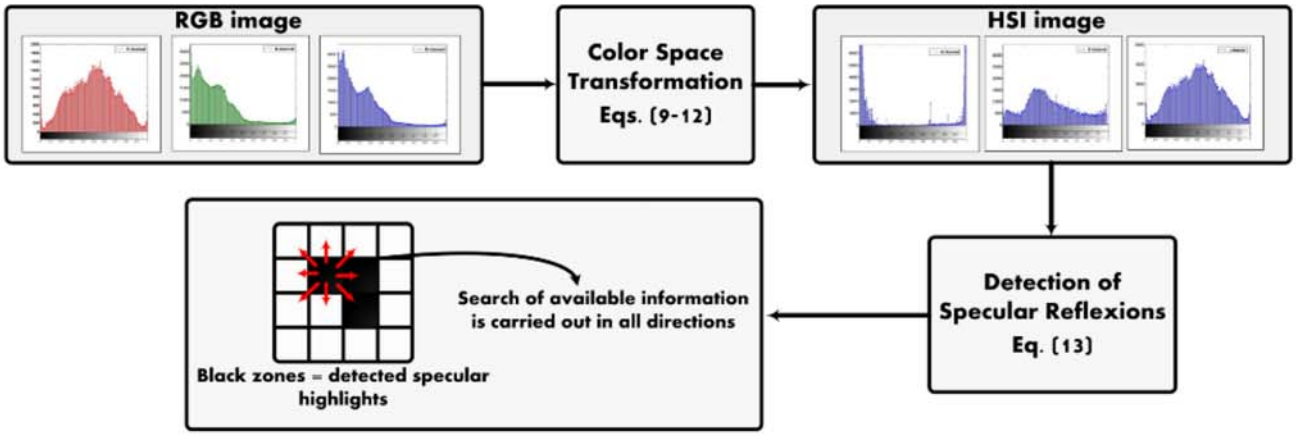

Fig. 4: Process applied in order to cope with specular highlights.

follows:

$$\mathbf{E_t(P)} = \frac{1}{2}\int_{\Omega} |(\mathbf{I_L}(\mathbf{d}(x)+x) - \mathbf{I_R}(x))|dx + \sum_{1}^{n}\int_{\Omega} |\nabla \mathbf{d}(x)|dx \tag{5}$$

From a practical point of view and efficiency, in this work the discretize-then-optimize methodology is used. Strictly speaking, taking original continuous functional from Eq. 4, it is rewritten by a discretization in order to obtain a standard optimization problem. Therefore, Eq. 5 is expressed as

$$\mathbf{E_t(P)} = \frac{1}{2}\sum_{x\in\Omega} |(\mathbf{I_L}(\mathbf{d}(x)+x) - \mathbf{I_R}(x))| + \sum_{1}^{n}\sum_{x\in\Omega} |\nabla \mathbf{d}(x)| \tag{6}$$

The main inconvenience of the previous formulation is that it is non-differentiable at zero. As a consequence, the optimization process is hindered, and standard methods are not directly applicable. A classic alternative is to use subgradient methods [38] or $\varepsilon-$subgradient methods [39], but they converge slowly and they have the lack of efficiency in certain cases. Another option is to treat the unconstrained non-differentiable problem as a constrained problem. The simplest and effective alternative is to redefine the functional with a differentiable approximation, allowing the use of classic unconstraint optimization methods. In this case, in order to avoid moving to the restricted area (i.e. zero), the log-barrier function given in Eq. 7 is applied, where $log(\cdot)$ is the natural logarithm and φ_+ is the value that determines the impact of the barrier over the function.

Let $\mathbf{f_{log}}$ be the logarithmic-barrier expressed by

$$\begin{aligned} \mathbf{f_{log}}(\mathbf{d}) &= -\varphi \sum_{x\in\Omega} log c_x(\mathbf{d}) \\ &\left\{\mathbf{d} \in \mathbb{R}^d | c_x(\mathbf{d}) > 0 \text{ for all } x \in \Omega\right\} \\ \nabla f_{log}(\mathbf{d}) &= -\sum_{x\in\Omega} \frac{\lambda}{c_x(\mathbf{d})} \nabla c_x(\mathbf{d}) \end{aligned} \tag{7}$$

In order to generate a differentiable approximation of the total energy Eq. 7 is integrated in Eq. 6 Therefore, the energy functional to be minimized becomes

$$\mathbf{E_t(P)} = \underbrace{\frac{1}{2}\sum_{\mathbf{x}\in\Omega} |(\mathbf{I_L}(\mathbf{d(x)}+\mathbf{x}) - \mathbf{I_R(x)})|}_{Ed} + \underbrace{\sum_{1}^{n}\sum_{\mathbf{x}\in\Omega} |\nabla \mathbf{d(x)}|}_{Er} \underbrace{- \varphi \sum_{x\in\Omega} log c_x(\mathbf{d})}_{f_{log}} \tag{8}$$

where $c_x = d^2$. Since the Eq. 8 becomes in a smooth minimization problem, it can be solved by a standard unconstrained methods. In this problem, Newton's method is applied to minimize Eq. 8, it has been selected due to its excellent global convergence.

3.3. Specular Highlights

Computational stereo methods are prone to error in presence of non-Lambertian specular highlights. In our case the surface properties of soft-tissue gives rise to specular reflections, which are the direct reflection of the light source on the glossy and wet-like surface. These specular reflections work as occluders and considerably reduce the available visual information used by the tracking algorithm. With the aim that two previous modules have a proper behaviour, the detection and removal of specular highlights must be carried out. So, to get rid of specular reflections, and increase the overall accuracy of the proposed tracking algorithm, a two-steps solution is presented (see Fig. 4) in which, after detecting regions affected by specular highlight, an inpainting process is applied in order to recover actual information of the heart surface.

Since specular reflections are characterized by local coincidence of intense brightness and unsaturated color [40], detection can be carried out by considering, and analyzing, these two color features. Although the saturation (S), and intensity (I) values can be directly obtained using the RGB (Red-Green-Blue) space, in our proposal the RGB image has been converted to the HSI (Hue-Saturation-Intensity) color-space. Three principal factors make this color-space ideal for developing computer vision applications [41]: its variables are somehow correlated with human being's color perception, decoupling the intensity component from the color information, and the close relationship between chromaticity and how humans perceive color. Among the existing RGB to HSI transformations, we have considered the given by Eqs 9 to 11 because is more robust to noise and the saturation component is made to be less sensitive to the nonlinear effects than in other transformations [42].

$$H = \begin{cases} \theta & \text{if } B \leq G \\ 360 - \theta & \text{si } B > G \end{cases} \tag{9}$$

$$\theta = cos^{-1} \left\{ \frac{\frac{1}{2}[(R-G)+(R-B)]}{[(R-G)^2+(R-B)(G-B)]^{\frac{1}{2}}} \right\} \tag{10}$$

$$S = 1 - \frac{3}{(R+G+B)}[\min(R,G,B)] \tag{11}$$

$$I = \frac{1}{3}(R+G+B) \tag{12}$$

Thus, saturation and intensity values of the image pixels are obtained using the above transformations, and then a specular detection solution based on thresholds is applied. This strategy is the most convenient due to its short computational time and its efficient detection. If I_m and S_m are the maximum intensity and saturation values of the pixels in the image, and $I^H \in \Omega$ denotes the regions showing specular reflections, we say that a pixel is in I^H if their intensity and saturation values (Int and Sat, respectively) satisfy the following condition:

$$\text{if}(Int > Th_{Int} \;\&\&\; Sat < Th_{Sat}) \text{ then belong to } I^H \tag{13}$$

where $Th_{Int} = 0.4 * I_m$ and $Th_{Sat} = 0.15 * S_m$ have been heuristically selected. Then, the image is converted to grayscale and all points in I^H are put in black color.

Once the specular regions have been determined the second step, inpainting, is applied. That is, given a region inside the domain of the image, inpainting is the process of modifying the image pixels' values in order to avoid standing out with respect of its surroundings [43]. The proposed inpainting process works as follows: the eight neighbors of the current position are taken, and only those who are different from black are used to calculate the mean. Finally, the result is assigned to the current position. This process is repetend until all positions are evaluated.

4. Experimental Results

This section illustrates the performance of the methodologies presented in Section III. Experiments have been conducted using a realistic data set from The Hamlyn Centre Laparoscopic [19]. The video sequence has a duration of 60.2 sec. in which the cardiac surface is affected by respiration and cardiac motion. Simulated experiments have been performed using a PC intel Core i7, 8GB RAM, and Nvidia GeForce GT 540M.

Firstly, in order to increase robustness and efficiency of the proposal specular highlights are taken into account, in Fig. 5 an example of the strategy

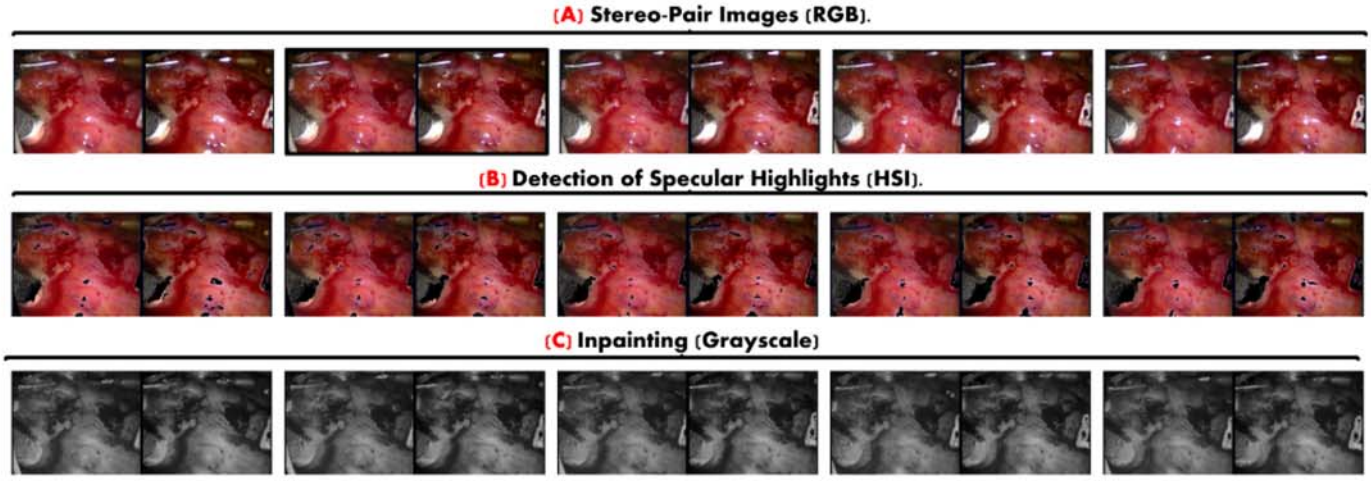

Fig. 5: (A) Part of the sequence of left and right original images, (B) Detection of the specular highlights using both attributes saturation and intensity in the HSI space color, (C) Reconstructed images using the proposed inpainting process.

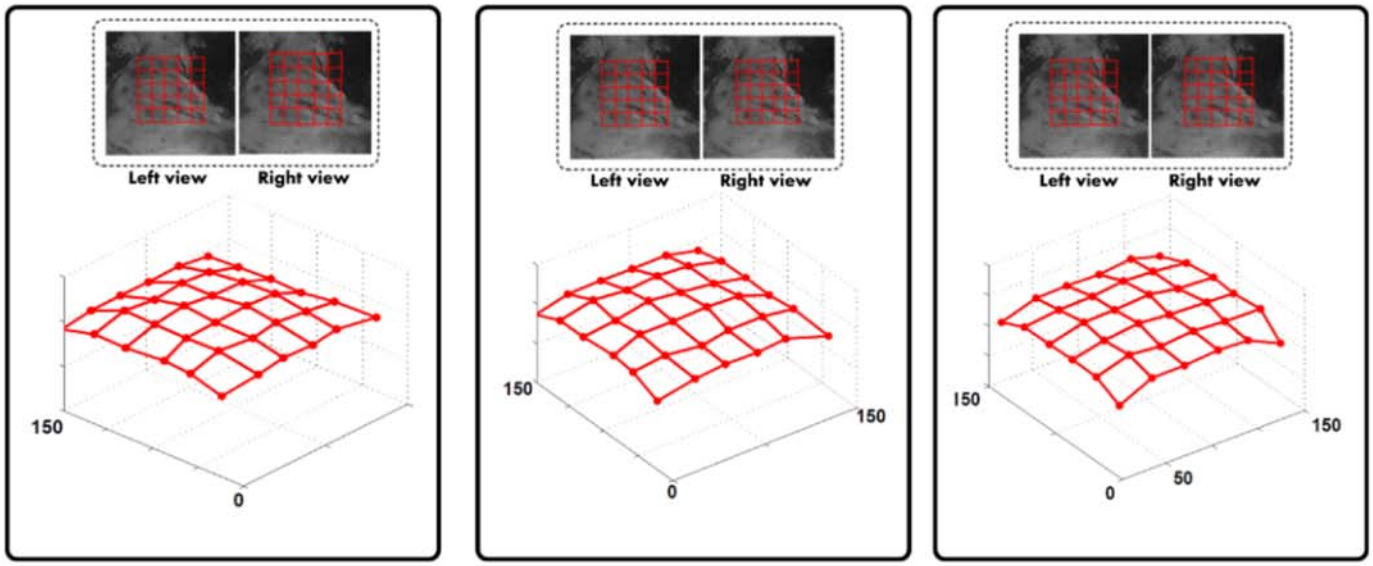

Fig. 6: Three dimensional world reconstruction, using the proposed approach, of three time instants of the image sequence (in pixels).

TABLE I: Performance Analysis

#Control Points	36
Avg. Time per stereo-pair [sec.]	0.0581
Avg. #Iterations per stereo-pair	19
Avg. Error Tracking (px)	1.25

presented in the subsection 3.3 is displayed, in which detection and inpainting of the specular highlights are carried out in order to avoid producing error during the execution of the proposed methodology. Moreover, it worth noticing that at the beginning of the approach, identification of the zone to be repaired is defined (see Fig. 7), and then, it is handled by a set of control points. In this case, 36 points were used because this number offer a good trade-off between a good approximation and short computational time. In

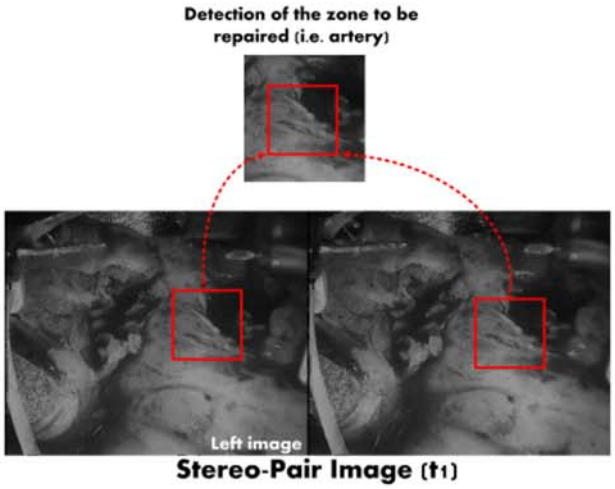

Fig. 7: Detection of the region to be repaired, i.e. the artery.

other words, as more points a better approximation is obtained but computational cost increases. In Fig. 6 the changes produced on the heart surface are shown in the three dimensional world, in which three time instants of the sequence are plotted. Moreover, it can be noticed that regularization term helps prevent unplausible deformation.

In order to validate the performance of the proposed approach, three main factors were evaluated: computational cost, i.e. average time per stereo-pair given in seconds; number of iterations during the optimization process given by the average number of iterations per stereo-pair; and accuracy evaluated by the average error of the tracking given in pixels. According with the results presented in Table I, the approach demonstrated to offer a good balance between accuracy and the computational time demand. Moreover, it demonstrated to work even during complex deformations.

5. Conclusions

In this work a new 3D methodology for physiological motion compensation during a robotic-assisted cardiac surgery has been presented. It is based on the $\ell 1-$regularized optimization class, in which deformation model is based on the cubic b-splines and the non-differentiability of the energy functional is coped via an approximation of it. Computational performance together with the accuracy, 0.0581 sec. and 1.25 px, demostraste the potential of the presented methodology even under complex deformations. As future work, this proposal will be combined with our methodology proposed in [44] for force estimation in order to avoid tissue damage.

Notation

$\mathbf{P}$: set of control point
$\mathbf{d}$: disparity
t : time
E_D : discrepancy energy
E_R : regularization energy
E_t : total energy
$\mathbf{f_{log}}$: logarithmic-barrier function
$\mathfrak{f}$: focal length
$\mathbf{I_L}$: left rectified image
$\mathbf{I_R}$: right rectified image
$log(\cdot)$: natural logarithm
n : number of dimensions
S : Saturation
I : Intensity
H : Hue
$\Upsilon_.$: basis functions
Ω : image domain
φ : barrier factor
ζ : regularization factor
∇ : gradient operator
x : vector
$\Re^+$: positive real numbers
$\mathbb{R}$: Set of real numbers

Acknowledgment

This work is supported by a FPU national scholarship from the Spanish Ministry of Education with reference AP2012-1943. Also, this work is part of the project DPI2011-29660-Co4-01 and DPI2011-29660-CO4-03 MINECO and with FEDER funds EC.

References

[1] J. Livesay, "The benefits of off-pump coronary bypass: A reality or an illusion?" *Texas Heart Institute Journal*, pp. 258–260, 2003.

[2] H. Broers and N. Jansing, "How precise is navigation for minimally invasive surgery?" *International Orthopaedics*, p. 3942, 2007.

[3] C. M. Gridley and H. T. Nguyen, "Ergonomics of laparoscopy," *Book Chapter Pediatric Endourology Techniques*, pp. 13–22, 2014.

[4] A. Lemma, A. Mangini, A. Redaelli, and F. Acocella, "Do cardiac stabilizers really stabilize? experimental quantitative analysis of mechanical stabilization," *Interactive CardioVascular and Thoracic Surgery*, 2005.

[5] M. L. Koransky, M. L. Tavana, A. Yamaguchi, M. H. Kown, D. N. Miniati, W. Nowlin, and R. C. Robbins, "Quantification of mechanical stabilization for the performance of off-pump coronary artery surgery," *Heart Surg. Forum, vol. 6*, pp. 224–231, 2003.

[6] I. Medtronic, "Fact sheet - octupus stabilizer tissue," *www.medtronic.com*, 2011.

[7] L. Maquet, "Fact sheet - identifying high-risk patients and improving cardiac surgery outcomes," *www.maquet.com*, 2012.

[8] S. Kinjo, J. Tokumine, K. Sugahara, M. Kakinohana, K. Iha, H. Matsuda, M. Akasaki, and Y. S., "Unexpected hemodynamic deterioration and mitral regurgitation due to a tissue stabilizer during left anterior descending coronary anastomosis in off-pump coronary artery bypass graft surgery," *Ann. Thorac. Cardiovasc. Surg., vol. 11*, p. 324328, 2005.

[9] R. Dzwonczyk, C. L. del Rio, C. Sai-Sudhakar, J. H. Sirak, R. E. Michler, B. Sun, N. Kelbick, and M. B. Howie, "Vacuum-assisted apical suction devices induce passive electrical changes consistent with myocardial ischemia during off-pump coronary artery bypass graft surgery," *Eur. J. Cardiothorac. Surg., vol. 30*, p. 873876, 2006.

[10] W. Bachta, P. Renaud, E. Laroche, A. Forgione, and J. Gangloff, "Design and control of a new active cardiac stabilizer. international conference on intelligent robots and systems." *International Conference on Intelligent Robots and Systems*, pp. 404–409, 2007.

[11] J. Gagne, W. Bachta, P. Renaud, P. O., Laroche, and J. Gangloff, "Beating heart surgery: Comparison of two active compensation solutions for minimally invasive coronary artery bypass grafting," *Book Chapter Computational Surgery and Dual Training Computing, Robotics and Imaging*, pp. 203–210, 2014.

[12] R. Ginhoux, J. Gangloff, M. de Mathelin, L. Soler, M.A.Sanchez, and J. Marescaux, "Active filtering of physiological motion in robotized surgery using predictive control," *IEEE Transactions on Robotics, vol.21, no.1*, pp. 67–79, 2005.

[13] O. Bebek and M. Cavusoglu, "Whisker sensor design for three dimensional position measurement in robotic assisted beating heart surgery," *IEEE International Conference on Robotics and Automation*, pp. 225–231, 2007.

[14] Y. Nakamura, K. Kishi, and H. Kawakami, "Heartbeat synchronization for robotic cardiac surgery," *International Conference on Robotics and Automation*, pp. 2014 – 2019, 2001.

[15] M. Sauve, A. Noce, P. Poignet, J. Triboulet, and E. Dombre, "Three-dimensional heart motion estimation using endoscopic monocular vision system: From artificial landmarks to texture analysis," *Biomedical Signal Processing and Control*, pp. 199 – 207, 2007.

[16] G. Kurz and U. Hanebeck, "Image stabilization with model-based tracking for beating heart surgery," *In proceeding on Jahrestagung der Deutschen Gesellschaft fr Computer- und Roboterassistierte Chirurgie*, 2012.

[17] E. Bogatyrenko, P. Pompey, and U. Hanebeck, "Efficient physics-based tracking of heart surface motion for beating heart surgery robotic systems," *International Journal of Computer Assisted Radiology and Surgery*, pp. 387–399, 2011.

[18] T. Ortmaier, M. Groger, D. Boehm, V. Falk, and G. Hirzinger, "Motion estimation in beating heart surgery," *IEEE Transactions on Biomedical Engineering*, pp. 1729–1740, 2005.

[19] D. Stoyanov, G. Mylonas, F. Deligianni, A. Darzi, and G. Yang, "Soft-tissue motion tracking and structure estimation for robotic assisted mis procedures," *In Proceeding Conference on Medical Image Computing and Computer Assisted Intervention*, pp. 139–146, 2005.

[20] B. Lo, A. Chung, D. Stoyanov, G. Mylonas, and G.-Z. Yang, "Real-time intra-operative 3d tissue deformation recovery," *IEEE International Symposium on Biomedical Imaging*, pp. 387–

1390, 2008.

[21] R. Richa, A. B, and P. Poignet, "Towards robust 3d visual tracking for motion compensation in beating heart surgery," *Medical Image Analysis*, vol. 15, no. 3, pp. 302 – 315, 2011.

[22] H. Elhawary and A. Popovic, "Robust feature tracking on the beating heart for a robotic-guided endoscope," *The International Journal of Medical Robotics and computer Assisted Surgery*, 2011.

[23] T. Ando, H. Kim, E. Kobayashi, H. Tsukihara, N. Motomura, S. Kyob, M. Onob, and I. Sakuma, "Simultaneous evaluation of wall motion and blood perfusion of a beating heart using stereoscopic fluorescence camera system," *Journal in Computerized Medical Imaging and Graphics*, pp. 276–284, 2014.

[24] B. Yang, W. Wong, C. Liu, and P. Poignet, "3d soft-tissue tracking using spatial-color joint probability distribution and thin-plate spline model," *Journal in Pattern Recognition*, pp. 2962–2973, 2014.

[25] B. Bayle, M. Joinie-Maurin, L. Barbe, J. Gangloff, and M. de Mathelin, "Robot interaction control in medicin and surgery: Original results and open problems." *Book Chapter in Computational Surgery and Dual Training*, pp. 196–191, 2014.

[26] A. Aviles and A. Casals, "Interpolation based deformation model for minimally invasive beating heart surgery," *Book Chapter IFMBE Proceedings vol.41, Springer International Publishing, 2013.*, 2013.

[27] A. Sotiras, C. Davatazikosy, and N. Paragios, "Deformable medical image registration: A survey," *Research Report Num. 7919, INRIA, France*, 2012.

[28] D. Tseng and J. Lin, "A hybrid physical deformation modeling for laparoscopic surgery simulation," *In proceedings of the 22 annual EMBS International Conference, Chicago IL*, 2000.

[29] F. L. Bookstein, "Principal warps - thin-plate splines and the decomposition of deformations," *IEEE Trans. Pattern Anal. Machine Intell.*, pp. 567–585, 1989.

[30] M. Davis, A. Khotanzad, D. Flaming, and S. Harms, "A physics-based coordinate transformation for 3d image matching," *IEEE Trans. Med. Imag.*, p. 317328, 1997.

[31] D. L. Collins and A. C. Evans, "Animal: validation and applications of nonlinear registration-based segmentation," *International Journal of Pattern Recognition and Artificial Intelligence*, p. 12711294, 1997.

[32] M. Unser, A. Aldroubi, and M. Eden, "The l2-polynomial spline pyramid," *IEEE Trans. Patter Anal. Mach. Intell.*, pp. 364–379, 1993.

[33] M. Unser, "Splines: A perfect fit for signal and image processing," *IEEE Signal Processing Magazine, vol.16, no.6*, pp. 22–38, 1999.

[34] J. Hadamard, "Lectures on the cauchy problems in linear partial differential equations," *Yale University Press, New Haven*, 1923.

[35] A. N. Tikhonov and A. V. Y., "Solution of ill-posed problems," *Winston and Sons, Washinton DC*, 1977.

[36] D. Mumford and J. Shah, "Optimal approximations by piecewise smooth functions and associated variational problems," *Communications on Pure and Applied Mathematics*, pp. 577–684, 1989.

[37] L. Rudin, S. J. Osher, and E. Fatemi, "Nonlinear total variation based noise removal algorithms," *Physica D., 60:259-268*, 1992.

[38] N. Z. Shor, "Subgradient methods: A survey of soviet research nonsmooth optimization," *Proceedings of the IIASA Workshop, Lemaréchal and R. Mifflin eds. Pergamon Press*, 1978.

[39] D. Bertsekas and S. Mitter, "A descent numerical method for optimization problems with nondifferentiable cost functionals," *SIAM Journal on Control*, pp. 637–652, 1973.

[40] T. Lehmann and C. Palm, "Color line search for illuminant estimation in real-world scenes," *Optical Society of America*, pp. 1271–1294, 2001.

[41] J. Keith, "Color spaces," *Book Chaper in Video Demystified*, pp. 15–34, 2007.

[42] R. Gonzalez and R. Woods, "Digital image processing," *Prentice Hall*, p. 299, 2001.

[43] V. C. M. Bertalmio, G. Sapiro and C. Ballester, "Optimal approximations by piecewise smooth functions and associated variational problems,"

Proceedings of the 27th annual conference on Computer graphics and interactive techniques, SIGGRAPH '00, pp. 417–424, 2000.

[44] A. Aviles, A. Marban, P. Sobrevilla, J. Fernandez, and A. Casals, "A recurrent neural network approach for 3d vision-based force estimation," *To appear in IEEE International Conference on Image Processing Theory, Tools and Applications*, 2014.